# SEI-component formation on sub 5 nm sized silicon nanoparticles in Li-ion batteries: the role of electrode preparation, FEC addition and binders†

Tony Jaumann,*[a] Juan Balach,[a] Markus Klose,[a] Steffen Oswald,[a] Ulrike Langklotz,[b] Alexander Michaelis,[b] Jürgen Eckert[ab] and Lars Giebeler[ab]

Silicon is a promising negative electrode for secondary lithium-based batteries, but the electrochemical reversibility of particularly nanostructured silicon electrodes drastically depends on their interfacial characteristics, commonly known as the solid electrolyte interface (SEI). The beneficial origin of certain electrolyte additives or different binders is still discussed controversially owing to the challenging peculiarities of interfacial post-mortem investigations of electrodes. In this work, we address the common difficulties of SEI investigations of porous silicon/carbon nanostructures and study the addition of a fluoroethylene carbonate (FEC) as a stabilizing additive as well as the use of two different binders, carboxymethyl cellulose/styrene-butadiene rubber (CMC/SBR) and polyacrylic acid (PAA), for the SEI formation. The electrode is composed of silicon nanocrystallites below 5 nm diameter allowing a detailed investigation of interfacial characteristics of silicon owing to the high surface area. We first performed galvanostatic long-term cycling (400 times) and carried out comprehensive *ex situ* characterization of the cycled nanocrystalline silicon electrodes with XRD, EDXS, TEM and XPS. We modified the preparation of the electrode for post-mortem characterization to distinguish between electrolyte components and the actual SEI. The impact of the FEC additive and two different binders on the interfacial layer is studied and the occurrence of diverse compounds, in particular LiF, $Li_2O$ and phosphates, is discussed. These results help to understand general issues in SEI formation and to pave the way for the development of advanced electrolytes allowing for a long-term performance of nanostructured Si-based electrodes.

## 1. Introduction

Lithium-ion batteries (LIBs) are currently the first choice for portable electronic devices due to their high energy density and good reversibility. For a significant further enhancement of the energy density, the development of new electrode materials with higher capacity is inevitable.[1,2] Silicon is a promising candidate to replace graphite as a commonly used anode in LIBs since it offers capacities up to 10 times higher than graphite and a low discharge potential. In addition, silicon showed high potential as a safe anode for future LIBs.[3–6] A critical aspect concerning silicon anodes is the so called "solid electrolyte interface" (SEI) which is a passive surface film typically formed on anode materials by decomposition of the electrolyte components

during the first cycle. If the SEI is stable, it prevents further decomposition of the electrolyte and allows good Li-ion conductivity. For instance, a graphite-based SEI formed during cycling in ethylene carbonate shows these positive properties which are a major reason for the extremely high reversibility of graphite as an anode.[7] This passive layer is supposed to be insufficiently stable on silicon due to continuous volume expansion and contraction of up to 300% during cycling.[8] The reiterating volume change causes a continuously growing passive interface which electrically isolates the active silicon species and results in fast capacity fading of silicon nanostructures whereas bulk silicon rather suffers from pulverization during lithiation. There are several strategies to stabilize the SEI on silicon. Liu *et al.* proposed a carbon encapsulation of silicon nanoparticles as an artificial SEI with void space between silicon and carbon to compensate the volume expansion.[9] Silicon nanoparticles below 20 nm seem to stabilize the SEI[10] due to highly reactive surface atoms which lead to the development of high-performance silicon nanostructures.[11,12] Another promising and facile approach that aims to stabilize the SEI formation on silicon is the use of electrolyte additives and modified conductive salts.[13–15] These modifications

[a] Leibniz Institute for Solid State and Materials Research (IFW) Dresden e.V., Institute for Complex Materials, P.O. Box 27 01 16, D-01171 Dresden, Germany. E-mail: t.jaumann@ifw-dresden.de; Fax: +49 351 4659 307; Tel: +49 351 4659 307

[b] Technische Universität (TU) Dresden, Institut für Werkstoffwissenschaft, Helmholtzstraße 7, D-01069 Dresden, Germany

† Electronic supplementary information (ESI) available. See DOI: 10.1039/c5cp03672k

24956 | *Phys. Chem. Chem. Phys.,* 2015, **17**, 24956–24967

This journal is © the Owner Societies 2015

can improve the reversibility exceptionally owing to the formation of a stable SEI during the initial cycles. One of the most promising candidates is fluoroethylene carbonate (FEC).[13,16,17] This compound drastically improves the cycle stability without complexly designed silicon structures. Intensive research has been carried out to determine the origin for the stabilization in order to design more efficient additives.[18] In this regard silicon nanowires,[19] thin silicon films[13,15,20–22] and silicon nanoparticles[23–25] with 50–100 nm in size have been examined. As the first group Choi *et al.* attributed the enhanced stability to a pronounced formation of LiF and Si–$F_x$ surface groups originating from the decomposition of FEC,[13] which was recently confirmed.[26] Other studies indicate the deposition of a smooth polycarbonate or a polymer-like layer on silicon as a main factor for stabilization.[18,20] A major reason for partially controversial results is found in the large number of parameters affecting SEI formation. Electrochemical preparation,[27] current rates[28] and potential windows for galvanostatic cycling significantly influence the SEI formation,[25] but more importantly, the procedures made for enabling post-mortem analyses.[27] The washing procedure of the electrode prior to analysis can affect the surface composition, but it is necessary to remove electrolyte components. The SEI on silicon typically consists of a complex structure with an upper organic layer (semi-organic lithium carbonates) and a lower inorganic matrix ($Li_2CO_3$, LiF, *etc.*).[24,25,29] In this regard, Tasaki *et al.* examined the solubility of different SEI components and showed that the organic salts can dissolve.[30] The dissolution of compounds may cause a huge variety of results in the literature. For example, the concentration of phosphorus, the central atom of the complex anion of the electrolyte's conductive salt, determined by X-ray photoelectron spectroscopy (XPS) on thin silicon films after cycling varies from 8 at% to 0.1 at% even under similar test conditions.[20,21] It is often ambiguous what is part of the SEI and what are just residues of electrolyte components like conductive salt $LiPF_6$ or solid co-solvents (*i.e.* ethylene carbonate). In addition, the role of the binder in the surface chemistry of silicon-based electrodes is not well investigated. It is believed that the functional groups of the binder (such as RCOOH) undergo chemical reaction with the silicon surface which should affect the surface chemistry.[31] To avoid these interactions binder-free electrodes are used for interfacial investigation, but their practical application is not realistic yet.[26,32,33] Therefore, an investigation with different binders will help to unveil their role in silicon-based anodes.

In this study, we highlight three current and delicate issues of SEI investigations for nano-silicon electrodes in Li-ion batteries: (I) the washing procedure for reliable post-mortem electrode characterization is addressed which is based on a short sonication treatment verified as an effective non-destructive procedure to remove only electrolyte components from the surface. (II) We focus on the superior electrochemical performance due to the addition of FEC and discuss the role of interfacial compounds in silicon electrodes, in particular $Li_2O$, LiF and phosphates formed during electrochemical cycling. (III) The significant effect of two well-known binders for silicon-based electrodes,

namely carboxymethyl cellulose/styrene-butadiene rubber (CMC/SBR)[31] and polyacrylic acid (PAA),[34] on SEI formation on nanoparticulate silicon is fundamentally investigated. As the Si anodes prepared with the help of the aforementioned binders show similar electrochemical performance and characteristics in the pristine state, post-mortem characterization identifies different organic surface species induced by just changing the binder. A model for the SEI formation is proposed and major challenges obtained in comparing the literature results under unique experimental conditions are discussed. We highlight the SEI properties and the SEI formation mechanism on silicon nanocrystallites with 2–5 nm in size embedded in a porous carbon scaffold after 400 galvanostatic cycles at high current rates for example for highly reversible and highly stable nanoparticulate Si-based negative electrode materials.

## 2. Experimental

### 2.1 Preparation of a silicon–carbon nanocomposite

A silicon–carbon nanocomposite was prepared according to a recently published synthesis procedure.[12] Briefly, a hydrogen silsesquioxane (HSQ) precursor was produced by polycondensation of trichlorosilane with water in the presence of a surfactant under an inert gas atmosphere. The dried HSQ precursor was annealed at 1100 °C which causes a transformation into a silica matrix with embedded silicon nanocrystallites of 2–5 nm in size determined by TEM and XRD.[12] After annealing, the composite was wrapped into carbon through carbonization of sucrose and finally etched with hydrofluoric acid to remove the silica matrix. The porous silicon–carbon nanocomposite (nc-Si@C) was dried under vacuum.

### 2.2 Electrochemical testing

A water-based slurry (8 : 1 : 1 = composite : Super P (TIMCAL) : CMC/SBR (1 : 1 m/m)) was prepared in 1 M HCl by using a swing mill and sonication. The temperature of the slurry should not exceed 25 °C in order to avoid oxidation. The electrodes were prepared by drop coating onto 12 mm copper discs (9 μm thickness, MTI Corporation) and subsequently dried under vacuum to minimize oxidation. Ethanol was used as solvent for the PAA binder (Sigma-Aldrich, $M_w \sim 450\,000$) to prepare the slurry (8 : 1 : 1 = composite : Super P : PAA). The final electrode was prepared by blade coating on copper foil and 12 mm copper discs were punched out. The mass loading was 2 ± 0.4 mg per electrode with about 33 wt% of total silicon on the electrode and a dried electrode thickness of 100 ± 9 μm. The electrodes were transferred into a glove box filled with argon ($H_2O$ < 1 ppm, $O_2$ < 0.1 ppm) and finally dried at 100 °C in a vacuum overnight before assembling Swagelok test cells. We used 250 μl of the electrolyte and a glass fiber (Whatman) as a separator for each cell. 1 M $LiPF_6$ in ethylene carbonate (EC) : dimethyl carbonate (DMC) with 1 : 1 v/v (LP30, Selectilyte BASF) was used as an additive-free electrolyte reference. The electrolytes containing the additive FEC (>99%, Solvay Chemicals) are composed of DMC : EC : additive (2 : 1 : 1 v/v/v) with 1 M $LiPF_6$

($>$99.9%, $<$20 ppm water, ABCR Chemicals). All chemicals were used as received without further purification. For the counter electrode metallic lithium foil (Chempur, 250 μm thickness) was applied. Galvanostatic cycling was carried out between 0.01–1.2 V vs. Li/Li$^+$ with a BaSyTec cell test system. All measurements were climatized at 25 °C. The specific capacity and current rates were calculated based on the mass of silicon. Investigations of the electrolyte decomposition were carried out in a three-electrode Swagelok cell, using lithium as counter and reference electrode and silicon–carbon nanocomposites as working electrodes. The experiment consisted of repetitive potentiostatic polarizations to 0.84 V vs. Li/Li$^+$ for a duration of one hour, and subsequent measurements of the open circuit potential over four hours.

### 2.3  Characterization of morphology

Prior to post-mortem characterization, the Swagelok cells were disassembled after 400 cycles in the glove box and the silicon electrodes were washed in 5 ml DMC ($<$20 ppm water, Selectilyte BASF) twice and once in 5 ml DMC in a sonication bath for 5 min, if not otherwise mentioned. For sonication, the samples were sealed in a container to avoid exposure to air/water and put into a continuous ultrasonic cleaner (VWR symphony). After sonication, the samples were kept overnight for sedimentation of the dispersed material, in order to remove the solvent. The electrodes were finally dried under vacuum for 1 h. The preparation for each characterization method was done in the glove box in order to avoid contact with air or moisture. X-ray powder diffraction (XRD) experiments were performed in transmission geometry with Cu K$_{\alpha 1}$ radiation on an STOE Stadi P diffractometer with a curved Ge(111) crystal monochromator and a 6°-position sensitive detector. The sample was pressed between Kapton tape to avoid exposure to air during scanning. The scan range was $10° < 2\theta < 90°$ with a step size of $\Delta 2\theta = 0.01°$ with three repetitions. Rietveld analyses were carried out assuming isotropic crystallite size distribution. Scanning electron microscopy (SEM) was realized with a Gemini 1530 from LEO equipped with a Bruker EDXS detector. TEM was performed using a Tecnai F30 equipped with a field emission gun and operated at 300 kV. A dispersion of the electrode material was dropped onto a copper grid with a lacey carbon film. During sample transfer into the electron microscope the exposure to air was minimized, but could not be completely excluded. X-ray photoemission spectroscopy (XPS) was carried out using a Physical Electronics PHI 5600 CI system with Mg Kα radiation (350 W) at a pass energy of 29 eV and a step size of 0.1 eV. The used Mg source (1253.6 eV) causes lower charging effects than a commonly monochromatic Al source (1486.6 eV) allowing a precise investigation of insulating SEI components. A special transfer chamber was used to prevent air exposure. The binding energies were normalized to LiF F 1s (685.5 eV) to correct for surface charging effects.[35] The pristine electrode was normalized to carbon C 1s (284.5 eV). Elemental concentrations from the XP spectra were calculated using standard single-element sensitivity factors. The core level signals were fitted with a Gaussian function (MagicPlot Software) using a basic linear background

after normalization to 1. Ar$^+$ sputtering was performed at 3.5 keV corresponding to 3.5 nm min$^{-1}$ for SiO$_2$. The silicon content in the nc-Si@C composite was determined by thermogravimetry (Netzsch Jupiter STA 449C) after combustion in synthetic air at 900 °C (10 °C min$^{-1}$ heating rate). From the amount of residual silica the silicon-to-carbon ratio was calculated.

## 3. Results and discussion

### 3.1  Properties of the pristine electrode

Structure and electrochemical performance of the porous silicon–carbon nanocomposite was extensively studied in our recently published report.[12] Herein, we address the surface properties of silicon after slurry-based electrode preparation which is crucial to understand the SEI formation on electrode materials in Li-ion batteries. In general, the hydride-terminated silicon nanoparticles at hand are meta-stable and slowly oxidize in air due to omnipresent radicals.[36] Thus, the surface properties of the silicon nanoparticles can change during the slurry-based electrode preparation in ambient atmosphere. To get an impression on the reactivity, surface species and structure of the nanoparticulate silicon are primarily characterized by XPS and XRD in order to evaluate structural changes during electrode preparation with the two different binders. The results are displayed in Fig. 1a which shows the typical X-ray diffraction pattern of cubic silicon. Data analysis according to the Rietveld method proves the presence of silicon nanocrystallites of less than 5 nm in size after preparation with water- (CMC/SBR) and ethanol-based (PAA) slurry. This observation is in agreement with the results for the as-synthesized nanocomposite.[12] The surface species were identified by XPS (Fig. 1b). In both samples, similar surface composition is observed as expected (Table S1, ESI†). The Si 2p binding energy position shows two maxima at 99.9 eV and 104 eV corresponding to silicon and silicon dioxide, respectively.[37] The binding energy position between these maxima is attributed to silicon suboxides. Both oxides are the result of silicon oxidation due to handling in air and the incomplete etching process of the silicon–carbon nanocomposite.[12,38] A native oxide layer is present on any silicon-based material and the high concentration of oxides in our material originates from the high surface area. Similar amounts of silicon dioxides and suboxides independent of the electrode preparation are found. Deconvolution of the C 1s binding energy shows peak maxima at 284.5 eV and 286 eV in both binders corresponding to C–C and C–O bonds, respectively, as a result of the porous carbon scaffold. Additional functional groups at 288–290 eV (ether, carboxy and carbonate groups) stem from the binder.

### 3.2  Electrochemical characterization

Electrochemical experiments were conducted in a conventional carbonate-based electrolyte composed of 1 M LiPF$_6$ in EC/DMC (1:1 v/v) (LP30) with and without partial substitution of EC with FEC (1 M LiPF$_6$) in EC/DMC/FEC (1:2:1 v/v/v) (LP30 + FEC) according to a recent publication.[16] The delithiation capacity vs. cycle number of the silicon–carbon nanocomposite depending
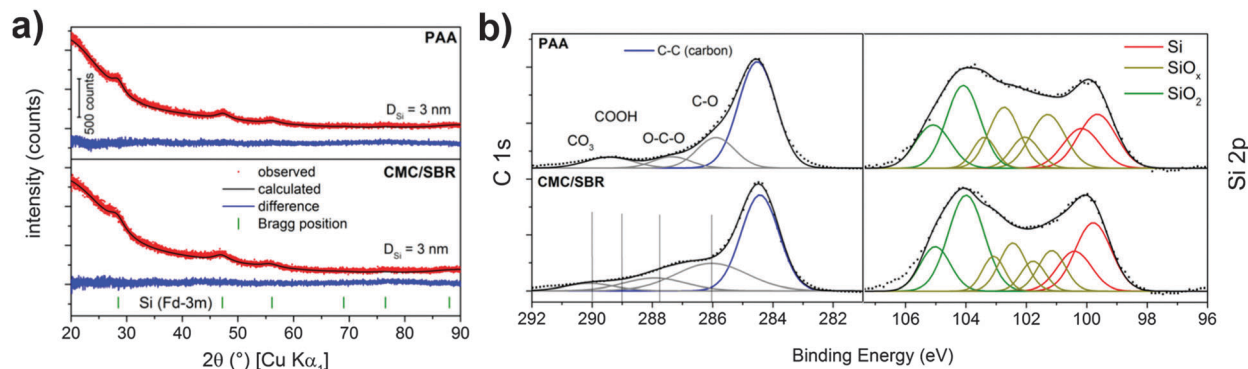
**Fig. 1** (a) XRD pattern and (b) XP spectra of the pristine silicon electrodes prepared with PAA and CMC/SBR as binders.
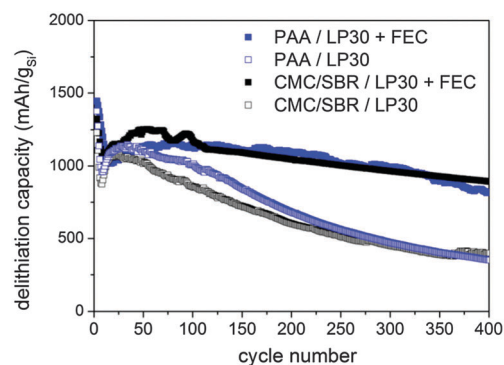


**Fig. 2** Galvanostatic cycling between 0.01–1.2 V vs. Li/Li$^+$ at 2.5 A g$^{-1}$ (two pre-cycles at 0.5 A g$^{-1}$) of the silicon electrode depending on binders and FEC addition.

on the two binders and the FEC addition is depicted in Fig. 2. The initial capacity is almost equal for all samples independent of binders and FEC addition. The initial drop and subsequent increase of capacity may be attributed to an activation process or to a delayed uptake of electrolyte into the porous structure.[39] This special behavior is not observed during cycling of the electrode at low current rates (0.5 A g$^{-1}$) confirming our assumption (Fig. S1a, ESI†). The largest difference in reversibility is observed depending on the FEC addition whereas the binder seems to affect the reversibility negligibly. However,

it will be shown that the results of SEI investigation vary depending on binders.

**3.2.1 FEC effects on the electrochemical performance.** With the addition of FEC the properties changed and the large differences occurring after FEC addition are addressed in detail. In the additive-free electrolyte the silicon anode reveals a capacity loss of 43% after 200 cycles and 75% after 400 cycles. In contrast, the addition of FEC stabilizes the silicon anode and causes a capacity loss of only 21% after 200 cycles and 36% after 400 cycles. Similar findings have been reported recently by using large silicon nanoparticles with sizes between 50–100 nm or structured silicon anodes.[16,19,22] As displayed in Fig. 3a, the Coulombic efficiencies (CEs) of the first cycles obtained from Fig. 2 are 35% with FEC and 40% for the additive-free electrolyte. A low CE suggests a severe initial SEI formation and strong electrolyte decomposition. However, after 10 cycles the CE reaches the highest value for FEC indicating a stabilized SEI on silicon. The same trend is observed at low current rates (Fig. S1b, ESI†), but with a higher CE already after the first cycle in the presence of FEC. Repetitive polarization experiments at 0.84 V vs. Li/Li$^+$ have been carried out to examine the electrolyte decomposition with and without FEC at the anode surface separated from the lithiation/delithiation (Fig. S2, ESI†). The results confirm the initial high consumption of FEC as deduced from the galvanostatic experiments and prove the formation of an extremely protective layer on the anode after cycling.
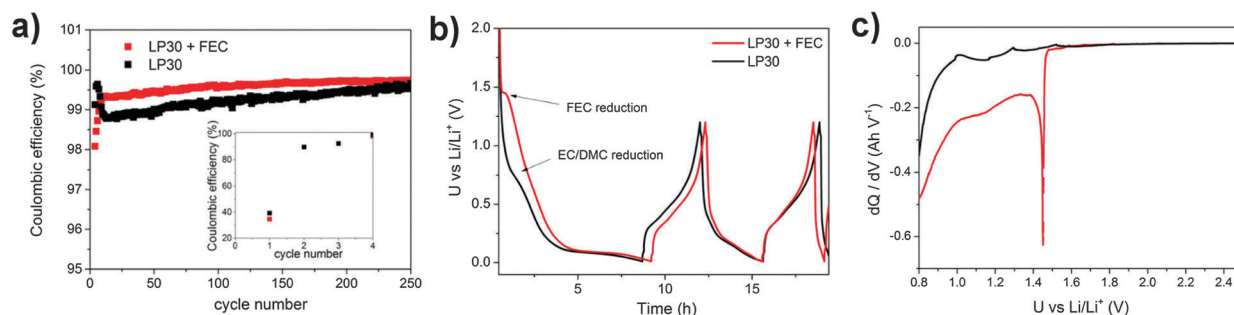


**Fig. 3** Electrochemical characterization of the silicon electrode with CMC/SBR as a binder depending on FEC addition. (a) Coulombic efficiency of the galvanostatic cycling between 0.01–1.2 V vs. Li/Li$^+$ at 2.5 A g$^{-1}$ (the first two cycles at 0.5 A g$^{-1}$), (b) the first two discharge/charge curves and (c) the differential capacity of the first discharge.

These results also confirm a recently published work,[26] but are contrary to other reports.[13,19] Fig. 3b shows the first two discharge/charge curves depending on the electrolyte. A flat voltage plateau at 1.45 V $vs.$ Li/Li$^+$ appears with FEC addition. This reduction current is better documented in the differential capacity profile d$Q$/d$V$ $vs.$ $U$ (Fig. 3c), a standard plot for the analysis of different reaction mechanisms in batteries, and indicates a two-phase transition likely as a result of FEC polymerization and precipitation on the high surface area of the electrode. In the case of the additive-free electrolyte, a slope below 0.9 V $vs.$ Li/Li$^+$ is attributed to the decomposition of ethylene carbonate. At potentials below 0.2 V $vs.$ Li/Li$^+$ the lithiation of crystalline silicon begins (Fig. 3b), exhibiting the characteristics of a two phase transition due to amorphization of the crystalline silicon.[24] These results are in accordance with the literature. Choi $et$ $al.$ reported a reduction of FEC at around 1.4 V.[13] Note that the two phase plateau of the FEC decomposition has not been described sufficiently in detail.[13,19] We attribute this distinct event to the sub-5 nm silicon nanocrystallites and the porous carbon scaffold. This nanostructured material exhibits a high surface area and thus causes stronger electrolyte consumption in the first cycle than observed in conventional silicon structures.[12,16]

### 3.3 Post-mortem analysis of the SEI

All electrodes were galvanostatically cycled 400 times between 0.01–1.2 V $vs.$ Li/Li$^+$ at a current rate of 2.5 A g$_{Si}^{-1}$ ($\sim$1 mA cm$^{-2}$) (shown in Fig. 2) and disassembled in the delithiated state.

**3.3.1 The removal of electrolyte components.** Before characterization of the SEI, compounds which are part of the SEI or which are residues of the electrolyte components have to be specified. Electrolyte components can hide or overlap the often

much weaker signals of SEI components. Identification of the origin of an enhanced reversibility caused by the SEI or its components are nearly impossible in this case. Typical electrolyte components which can be found as residues are EC, FEC and the conductive salt LiPF$_6$. It is well-established in the literature to wash the silicon electrode smoothly 1–3 times with dimethyl carbonate (DMC) in order to remove the electrolyte components, but typically considerable amounts of the conductive salt are observed.[21,22,25,40] For thin silicon films[20] simply washing of the electrode may be sufficient because the surface is low, but for often studied porous silicon–carbon nanocomposites with a high surface and sometimes high pore volume (as in our case) considerable amounts of electrolyte components can still remain after smooth washing[19,24] due to the high absorbing capabilities. Thus, we applied a short sonication procedure to remove loose electrolyte components. In order to show the suitability of this technique as non-destructive for SEI components for the removal of electrolyte components, we characterized one electrode after rinsing three times with DMC and an identically cycled electrode with an additional sonication process of 5 min in the third and final washing process. The results of XPS are presented in Fig. 4. With sonication, the silicon concentration increases and the phosphorus as well as fluorine concentration is lower as expected for the removal of electrolyte components. The same trend is observed for measuring the electrode composition with EDXS (Table S2, ESI†). Considering the binding energies of each element (Fig. 4 and Li 1s/O 1s are shown in Fig. S3, ESI†) before and after sonication, we can observe only two major differences:

(1) From deconvolution of the P 2p spectrum, we determined 0.08 mol% LiPF$_6$ with sonication and almost three times more without sonication (0.24 mol% LiPF$_6$). The occurrence of LiPF$_6$
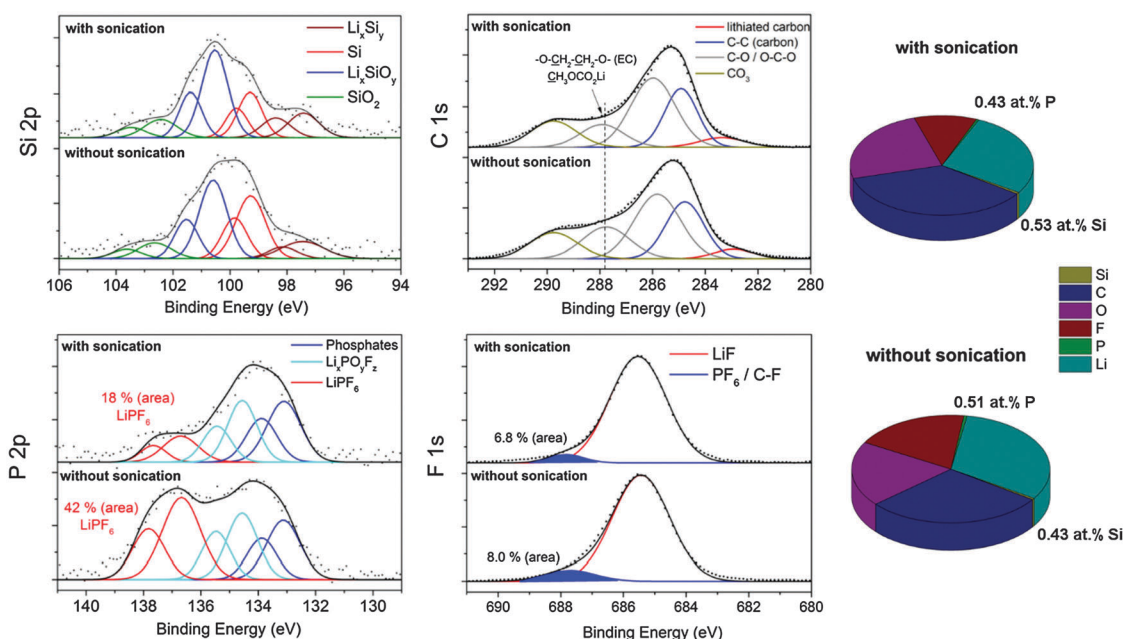


**Fig. 4** XP spectra (left) and concentration (right) of the silicon electrode with PAA as a binder after 400 times cycling in LP30 with FEC addition depending on the washing procedure (washed 3 times in DMC with a final sonication process or 3 times in DMC without sonication).

compounds is verified by the appearance of a binding energy position at ∼688 eV in the F 1s spectrum.

(2) The binding energy position at ∼288 eV in the C 1s spectrum decreases by approximately 20% after sonication which we majorly attribute to a lowered O–$CH_2$–$CH_2$–O/O–CHF–$CH_2$–O concentration originating from EC/FEC and to the partial removal of easily soluble semi-organic carbonates such as ($CH_2OCO_2Li$)$_2$, $CH_3OCO_2Li$ as typical upper SEI components.[30,41] The removal of these components is also be observed in the O 1s spectrum (Fig. S3, ESI†) because the intensity of the binding energy position at 534 eV corresponding to C–O species is lowered after sonication. Note that the concentration of the $CO_3$ (290 eV) and C–O (286 eV) species is nearly equally independent of the washing procedure indicating retained $Li_2CO_3$ and $CH_3$–OLi.[41]

All other elements show no change in their chemical characteristics. Importantly, the Si 2p spectrum is higher resolved after sonication due to the higher concentration of silicon and the binding energies remain constant indicating a leftover of reaction-sensitive Si/$Li_xSi_y$ nanoparticles during the washing procedure. Phosphates ($PO_x$) are a major part of the SEI whereas $PF_6$ species seems to be mainly a residue of the electrolyte. Although it was proposed that $LiPF_6$ may be part of the SEI,[25] our results show that this species is easily soluble and likely dissolves during cycling whereas the vast majority of $CO_x$ species and phosphates remain. Hence, $PF_6$-containing compounds cannot be substantial part of the SEI on small-sized silicon nanoparticles. In summary, a short sonication procedure is a promising non-destructive way to remove softly-bond electrolyte components. However, the partial removal of the upper organic SEI components (in particular $CH_3OCO_2Li$) cannot be excluded, but it allows characterization of the interfacial characteristics of silicon and the upper organic SEI and is a suitable technique for non-destructive depth-profiling of the SEI.

**3.3.2 FEC effects on SEI formation.** For clarity, we applied the sonication procedure to remove any electrolyte components. EDXS (Table 1) provides valuable information of the elemental composition of the entire post-mortem electrode. It reveals the lowest silicon and highest carbon content cycled in the additive-free electrolyte suggesting pronounced decomposition of electrolyte components. For the additive-containing electrolyte an increase of silicon concentration from approximately 7 wt% to about 10 wt% and a lower carbon concentration are observed. This result points to less organic material and thus weaker decomposition of the electrolyte. A significant difference is detected for the fluorine concentration which is eight times higher in the presence of FEC as electrolyte additive. A larger amount of additive decomposed during cycling is

concluded from these observations and is also in accordance with recent reports.[18,20] Interestingly, considerable amounts of phosphorus are only present when FEC is used.

X-ray diffraction gives insights about structure and morphology of the entire post-mortem electrode and the results are depicted in Fig. 5. No reflections appear in the case of the additive-free sample, indicating a completely amorphous material. Note that the silicon reflections typically disappear after cycling due to an amorphization process during lithiation.[42] In the case of FEC, we observe the reflections of LiF with a cubic crystal structure ($Fm\bar{3}m$). From the XRD pattern a crystallite size of roughly 4 nm is determined by Rietveld analysis. The formation of crystalline LiF is also confirmed by TEM (Fig. 5b). The bright-field images show an agglomeration of the porous carbon scaffold attached to silicon nanoparticles after cycling. A high-resolution analysis is impossible because the high-energy electron beam decomposes the SEI components. However, selected area electron diffraction (SAED) proves the formation of nanocrystalline LiF only for the addition of FEC. LiF is often detected by XPS measurements, but has not yet been reported in diffraction experiments after cycling. It is likely formed in the initial cycles where a two-phase transition is observed which suggests a precipitation from the liquid phase. The role of fluorides in Li-ion batteries is
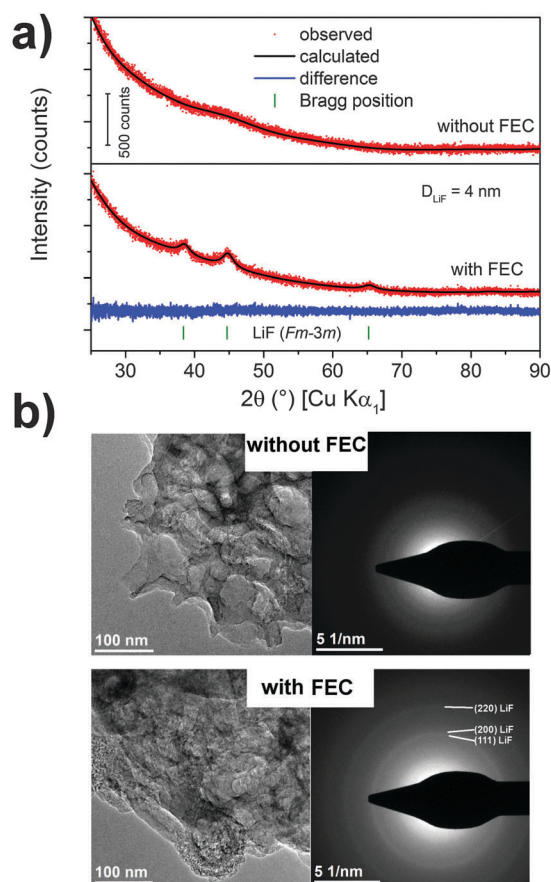
**Fig. 5** (a) XRD pattern and (b) TEM bright–field images (left) with selected area electron diffraction (SAED) (right) of the cycled silicon electrodes with CMC/SBR depending on FEC addition.

**Table 1** Elemental composition of the silicon electrode with CMC/SBR as a binder after 400 time cycling depending on FEC addition determined by EDXS

| Sample | Si (at%) | C (at%) | O (at%) | F (at%) | P (at%) |
|---|---|---|---|---|---|
| w/o FEC | 6.8 | 42.1 | 48.8 | 2.2 | 0 |
| With FEC | 10 | 37.8 | 39.5 | 11.1 | 0.7 |

This journal is © the Owner Societies 2015

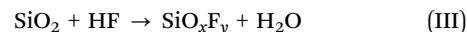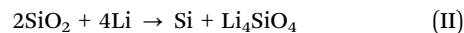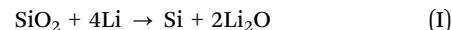*Phys. Chem. Chem. Phys.*, 2015, **17**, 24956–24967 | **24961**

controversially discussed.[43] LiF is recognized as an insulator for both lithium ions and electrons and its formation should be avoided.[44] In contrast to this, LiF is often associated, among other compounds, as a SEI-stabilizing component for silicon-based electrodes resulting in an enhanced cycling stability.[13,26,45,46] The rather controversial literature reports suggest that LiF may be neither beneficial nor disadvantageous for the reversibility. From the aspect of diffraction experiments, we can detect LiF only in the presence of FEC. From this point of view LiF indeed supports a better cycling stability. However, since most of the material is amorphous, further information for evaluation is provided by XPS measurements.

Fig. 6 displays the XPS results and the chemical composition. We detect a concentration of ∼1 at% silicon for both samples. Higher amounts of lithium in the FEC sample indicate lithium salts as major components of the interfacial layer on silicon. Further differences are found in the carbon/oxygen ratio and the fluorine concentration. With FEC the carbon/oxygen ratio is higher (1.31) than without additive (0.8). The fluorine and phosphorus concentration is up to five times higher with FEC suggesting high decomposition of the additive and an integration of hydrolysis products of LiPF$_6$ into the SEI. Higher amounts of phosphorus with FEC addition were reported by Elazari et al. and Chen et al. on, respectively, thin silicon films and silicon nanoparticles, suggesting pronounced decomposition of the conductive salt as well as the integration of the products into the SEI.[17,22] However, almost no phosphorus is detected without the additive.

Both Si 2p spectra in Fig. 6 show signals with a maximum at approximately 101 eV which correspond to Li$_x$SiO$_y$.[24] This compound is an initial reaction product of lithium with SiO$_2$ which is present in large concentrations on the pristine electrode (Fig. 1).

From literature[24] it is known that SiO$_2$ undergoes different reactions during cycling which are summarized here:

$$SiO_2 + 4Li \rightarrow Si + 2Li_2O \quad (I)$$

$$2SiO_2 + 4Li \rightarrow Si + Li_4SiO_4 \quad (II)$$

$$SiO_2 + HF \rightarrow SiO_xF_y + H_2O \quad (III)$$

The release of HF is a by-product of the reaction of the PF$_6^-$ ion with traces of water and the decomposition of the FEC additive. From reactions (I)–(III), it is clear that large amounts of both Li$_2$O and Li$_4$SiO$_4$ can be formed during the first discharge process which was reported by Philippe et al.[25] For the additive-free sample we additionally observe a shoulder at 105 eV which corresponds to fluorinated silicon suboxides (SiO$_x$F$_y$)[25] and SiO$_2$. SiO$_2$ may partially be the result of residues from the glass fiber separator. Considering the sample cycled in the FEC-containing electrolyte, an additional elemental silicon signal at 99 eV is present which corresponds to the active material for reversible lithium storage. By fitting each silicon species we determined an elemental silicon contribution of approximately 23% whereas the additive-free sample shows less than 10%. This observation suggests a very thin initial SEI of less than 4 nm in the case of additional FEC since the XP attenuation length of laboratory X-ray sources (here, 1253.6 eV energy) is around 2–3 nm.

The total amount of carbon–oxygen (CO$_x$) species on the pristine electrode was estimated to be 34%. After cycling in the additive-free electrolyte the C 1s binding energy position features a maximum at 285.7 eV majorly corresponding to C–O species and to conductive carbon (C–C species at 284.5 eV).[47] A second local maximum at 290 eV is observed caused by lithium
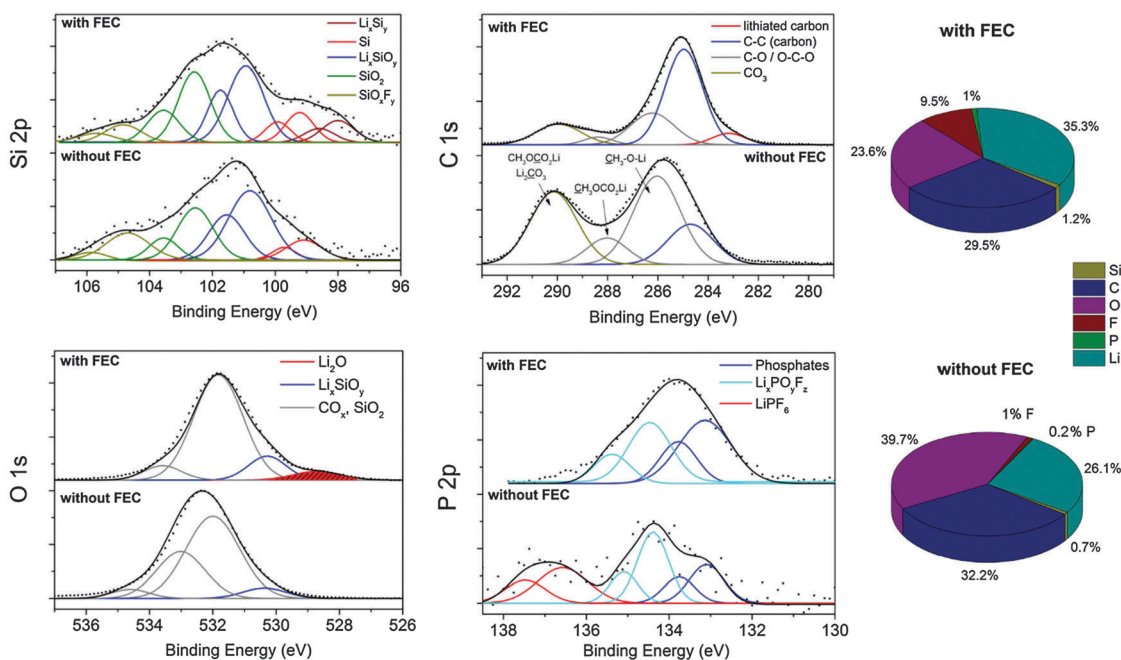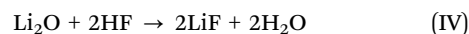


Fig. 6  XP spectra and concentrations of the silicon electrodes with CMC/SBR as a binder cycled 400 times depending on FEC addition.

carbonates and diverse semi organic lithium carbonates. These results evidence the presence of $(CH_2OCO_2Li)_2$, $CH_3OCO_2Li$, $CH_3OLi$ and $Li_2CO_3$ as typical SEI components in alkyl carbonates.[41] The total amount of $CO_x$ species increased to 83% indicating a strong electrolyte decomposition. With FEC as an additive the dominant signal is shifted to 284.9 eV which majorly corresponds to the conductive carbon scaffold as a result of the thin SEI. The low energy signal at 283 eV corresponds to lithiated carbon.[48] Only low amounts of $CO_3$ and C–O species with a total concentration of 39% are present which is only slightly higher than for the pristine electrode (34%). This observation provides the proof of a negligible decomposition of the electrolyte solvents DMC and EC. The low concentration of $CO_3$/C–O species and the high intensity of C–C/C–H bonds point to the formation of a thin layer-like polymer, presumably a vinyl polymer with functional C–O/$CO_3$ groups, on the silicon–carbon composite. It was proposed that FEC can decompose to HF and vinylene carbonate which oligomerizes to polycarbonates as the stable SEI on silicon.[19] Vinylene carbonate has been proven to be an effective stabilizer in LIBs owing to the formation of stable polycarbonates.[49] Nakai et al.[20] proposed HF and $Li_2CO_3$ formation by a ring opening reaction of FEC and its subsequent polymerization to a vinyl polymer. A recent report[17] suggests the formation of poly(-vinyl carbonates).

The binding energy position of the Li 1s core level spectra (Fig. S4, ESI†) is located at about 56 eV for both samples and corresponds to various lithium salts in the SEI.[48] The characteristics in the O 1s spectrum are similar. For the additive-free a peak maximum at 532.5 eV is observed. The addition of FEC shifts this peak maximum to lower energies (531.5 eV). Higher energies indicate the presence of more $CO_x$ species whereas the lower O 1s binding energy position is attributed to the presence of $Li_xSiO_y$ which is supposed to be a major component of the SEI on silicon.[24] Taking into account the integrated peak area and the silicon/oxygen concentration, we determined a stoichiometric oxygen number of about 3 for the additive-free sample and 4 with FEC according to reaction (II). Interestingly, we observe a peak maximum at 528.5 eV only in the FEC sample which corresponds to $Li_2O$. $Li_2O$ is typically formed in the first cycle due to the reaction of $SiO_2$ with lithium, as explained earlier (reaction (I)). Philippe et al.[24] reported that $Li_2O$ was reversibly detected in nano-silicon anodes even after many

cycles but seems to disappear owing to a dissolution by HF from the decomposition of FEC and $LiPF_6$:

$$Li_2O + 2HF \rightarrow 2LiF + 2H_2O \qquad (IV)$$

To further investigate the presence of $Li_2O$, we sputtered the sample for 5 min in order to remove the first 15–20 nm of the surface. Although sputtering is known as a destructive method, it does not necessarily destroy all chemical compounds in the SEI. Previous investigations of metallic lithium anodes show that $Li_2O$ is stable during sputtering with an $Ar^+$ beam.[50] After sputtering (Fig. 7), the $Li_2O$ peak in the O 1s spectrum appears significantly more intense in the case of the FEC sample. In contrast, no $Li_2O$ is observed in the sample cycled in the additive-free electrolyte. Note that $Li_2O$ can also be formed by decomposition of lithium carbonate by $Ar^+$ sputtering. However, if this reaction occurs, $Li_2O$ will be predominantly present in the additive-free electrolyte due to the higher amount of carbonates in the SEI. The results indicate that $Li_2O$ must be located between the silicon and the upper SEI and can be retained with FEC addition. We will also consider the C 1s energy (Fig. 7) after sputtering to show that the results for carbon species are reasonable. The peak maximum is shifted to lower energies as a result of the partially uncovered carbon scaffold and residues of lithiated carbon in both samples. Furthermore, the amount of $CO_x$ compounds decreases due to the removed SEI matrix. These observations agree well with results from non-destructive depth-profiling.[24,48] Based on this observation, we propose that the thin SEI formed with FEC is sufficiently stable to prevent the dissolution of $Li_2O$ by HF. This result is surprising since HF readily diffuses through any thin polymer. The SEI formed with FEC effectively suppresses HF diffusion and is chemically very stable. This property of the SEI is in accordance with a recent study which proved good thermal stability of the SEI formed with FEC of up to 200 °C on highly reactive lithiated silicon.[23] Another study reports an enhanced reversibility for nano-silicon anodes with the conductive salt lithium bis(fluorosulfonyl)imide (LiFSI) as well.[14] Similar to FEC, the dissolution of $Li_2O$ was successfully suppressed here but could be rather a result of a weaker HF generation from the more stable LiFSI salt (compared to $LiPF_6$) than from a protective layer. However, it suggests that an inhibited dissolution of
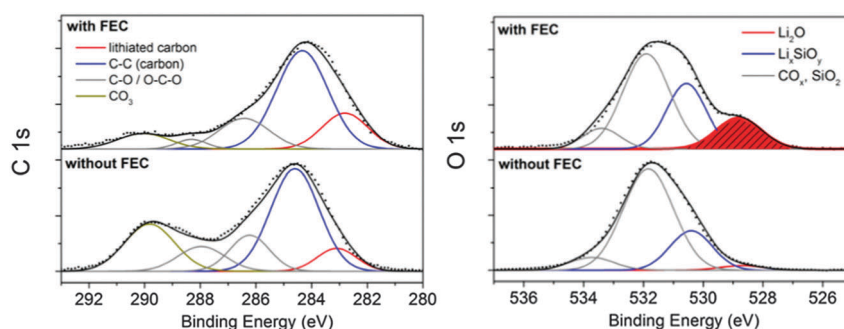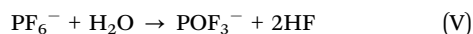


Fig. 7 XP spectra of the silicon electrodes with CMC/SBR as a binder cycled 400 times depending on FEC addition after $Ar^+$ ion sputtering (~15 nm surface removal).

Li$_2$O and its formation from silicon dioxide may be a good indication for better cycle stability.

The F 1s spectrum (Fig. S5, ESI†) of the additive-free sample in the non-sputtered state consists of a signal at 687.7 eV with low intensity and a distinct signal at 685.5 eV corresponding to traces of LiPF$_6$, Li$_x$PO$_y$F$_z$ and LiF, respectively. The phosphorus species are confirmed by the P 2p spectrum (Fig. 6). The signal at 137.5 eV points to traces of the conductive salt and the one at 134.5 eV to partially fluorine-substituted phosphates (reaction (V)). The presence of fluorine-substituted phosphates as part of the SEI after cycling in a conventional carbonate-based electrolyte has been reported previously.[19,22,25] The concentrations of these phosphates seem to vary noticeably. Our results suggest that negligible concentrations of partially fluorinated phosphates participate in the SEI formation on silicon in the additive-free electrolyte. With addition of FEC, the F 1s spectrum exhibits solely one signal at 685.5 eV corresponding to (nanocrystalline) LiF as already confirmed with XRD. The LiF cannot be present as a closed layer since a crystallite size of 4 nm (determined by diffraction experiments) in a layer-like structure would cause the absence of any other signal in the XP spectrum as a result of the low attenuation length of these photons (2–3 nm) at this energy. Thus, the overall morphology of LiF is present as nanoparticles or as a fragmentary scaffold. This finding contradicts a recent work suggesting that a layer-like structure of LiF stabilizes the SEI.[26] Our findings support other reports attributing the enhanced reversibility to an organic polymeric film structure.[40] The P 2p spectrum (Fig. 6) reveals a binding energy position at 134.0 eV proving the presence of majorly phosphates and fluorine-substituted phosphates. The presence of FEC causes the hydrolysis of considerable amounts of LiPF$_6$ to (fluorinated) phosphates which are integrated into the inorganic part of the SEI. The general reaction path of the phosphate formation was described in literature.[25] (reaction (V)).

$$PF_6^- + H_2O \rightarrow POF_3^- + 2HF \qquad (V)$$

Hence, more water is generated in the presence of an additive, which may be formed by the reaction of silica and Li$_2$O with HF (reaction (III) and (IV)). Latter is generated by the decomposition of the fluorine additive. Similar results were reported by Choi et al.[13] and Elazari et al.[22] on thin silicon films. Hydrolysis of PF$_6^-$ ions is considered as a major factor for irreversible capacity loss in LIBs, but it seems to influence the electrochemical performance positively. This behavior is consistent with a report of Dalavi et al.[15] who observed a positive effect for the incorporation of decomposed LiPF$_6$ into the SEI. However, in a recent study dealing with silicon nanoparticles ($>50$ nm) less decomposition of PF$_6^-$ was observed when FEC is added.[40] This observation may result from less silicon dioxide on large silicon nanoparticles which is considered as a major reason for a pronounced water generation (reaction (III)). We propose that the amount of silicon dioxide plays a critical role in cycle retention. It was shown that a certain amount of silicon dioxide can stabilize the electrochemical performance.[51] This finding likely correlates with the observed Li$_2$O and phosphates which are the successive reaction product of silicon dioxide on the pristine electrode surface with the electrolyte.

**3.3.3 The effect of the binder.** To study the effect of the binder on the SEI formation, we used the electrolyte LP30 with FEC addition. For both binders a thin SEI on silicon is found because significant amounts of elemental silicon are observed in the Si 2p spectrum (Fig. 4 and 6). This characteristic was observed only with FEC addition and is independent of the binder. However, the concentration of silicon is considerably less when PAA is used as binder (Table 2) which lowers the resolution of the Si 2p spectrum.

In addition, the carbon and fluorine concentration is higher and the C 1s energy (Fig. 8a) reveals significantly more CO$_x$ compounds on the surface with PAA as binder. In particular, the concentration of DMC/EC and their related compounds increases considerably whereas the lithium concentration is considerably lower with PAA suggesting lower proportions of lithium salts as major constituents of the SEI. The Li$_2$O identified as retained interfacial compound with FEC addition is solely observed after sputtering (Fig. 8b) indicating a thicker passive layer with the PAA binder. The P 2p spectrum reveals higher concentration of LiPF$_6$ with the PAA binder (Fig. 4 and 6). From these results, we conclude that the overall chemical species in the SEI are similar, but the amount of electrolyte-related components such as EC/DMC and LiPF$_6$ is higher when PAA is used. This observation may be the result of a stronger interaction of electrolyte components with PAA, for instance with a pronounced swelling in the electrolyte since PAA is a well-known superadsorber. Magasinski et al. analyzed the swelling of PAA and CMC and found no significant difference.[34] However, they used diethyl carbonate (DEC) whereas the smaller molecule DMC as solvent in LP30 may behave differently. Furthermore, the analyzed molecular weight was considerably lower. Our assumption is supported by a study of Bordes et al. dealing with nano-Si/graphene in PAA as a binder cycled in LP30 with FEC.[18] The test conditions and electrode composition were comparable to the conditions chosen for our work. They observed no silicon on the electrode surface by XPS after 50 cycles[18] which is conform to our study since only little concentration of silicon was observed with PAA. In conclusion, a different binder does not change the overall structure of the SEI, but it can considerably change the amount of surface species on the electrode which originates from the swelling of the binder with electrolyte as well as stronger or weaker interactions of electrolyte-related components with the individual binder. It can impede the detection of crucial SEI components due to a thicker layer of electrolyte(-related) species on the electrode surface, as shown for Li$_2$O as a typical interfacial SEI component on silicon.

**Table 2** Elemental composition of the silicon electrode determined by XPS after 400 time cycling in LP30 with FEC addition depending on the binder

| Sample | Li (at%) | Si (at%) | C (at%) | O (at%) | F (at%) | P (at%) |
|---|---|---|---|---|---|---|
| CMC/SBR | 35.23 | 1.17 | 29.44 | 23.57 | 9.48 | 0.95 |
| PAA | 27.55 | 0.53 | 36.08 | 24.32 | 11.09 | 0.43 |

**24964** | *Phys. Chem. Chem. Phys.,* 2015, **17**, 24956–24967
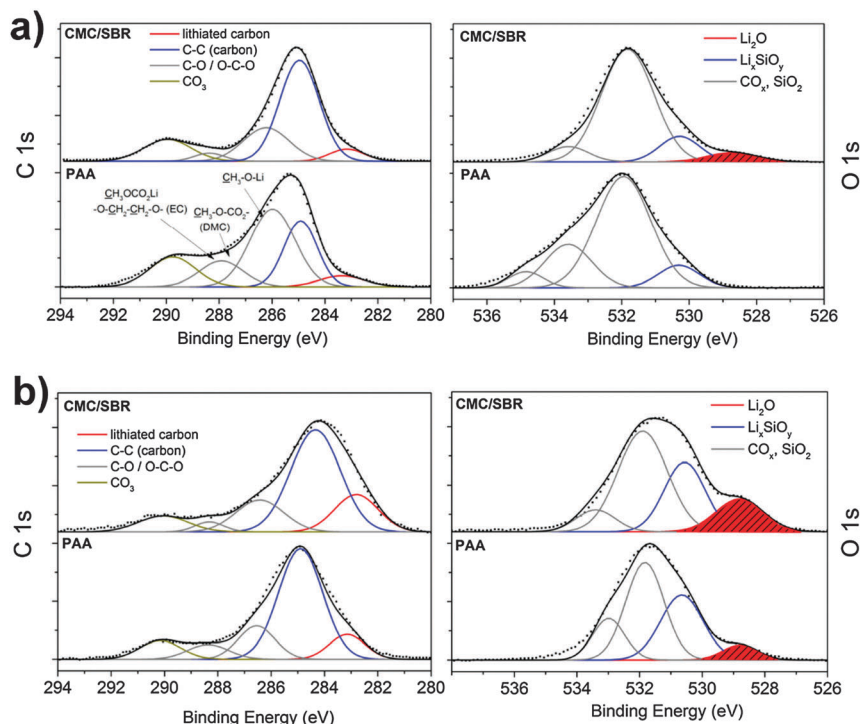
This journal is © the Owner Societies 2015

**Fig. 8** XP spectra of the silicon electrodes cycled 400 times in LP30 with FEC depending on the binder (a) no sputtering and (b) after sputtering with an Ar$^+$ beam (~15 nm surface removal).

# 4. Conclusion

The electrochemical analysis of the nanocrystalline silicon/carbon electrode with FEC addition revealed an enhanced reversibility, but initially a higher electrolyte consumption compared to the additive-free electrolyte. After a few cycles the decomposition with FEC addition is negligible suggesting the formation of a protective layer. The CMC/SBR or the PAA binder does not influence the overall electrochemical performance. Galvanostatic long-term cycled electrodes (400 times) were characterized depending on FEC addition and binders. A modified washing procedure of the electrodes including a sonication step was investigated which allows the evaluation of the actual SEI and residues of electrolyte

components appearing very similar to that specified by common surface sensitive characterization techniques. The results suggest that retained LiPF$_6$ salt plays a negligible role in the SEI of silicon/carbon electrodes. The addition of FEC causes an extremely low electrolyte decomposition (EC/DMC) even after 400 cycles. The formation of considerable amounts of nanocrystalline LiF was observed by XRD, TEM and XPS. The crystallite size of 4 nm suggests a particle-like rather than a closed film-like morphology. From this result we propose that fluorides have neither a beneficial nor a disadvantageous effect on the reversibility and are just decomposition by-products at most. We attribute the enhanced reversibility with FEC to a very thin (<4 nm) polymer layer (presumably a vinyl polymer) on the silicon/carbon electrode.
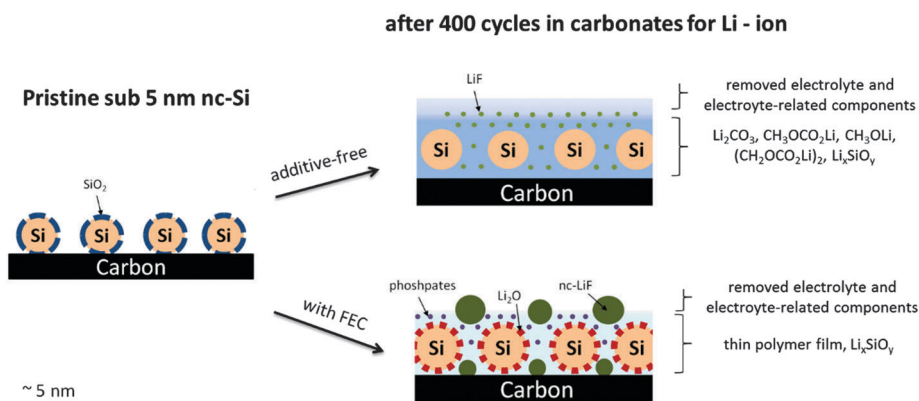


**Fig. 9** Simplified schematic illustration of the silicon–carbon nanostructure after long-term cycling depending on FEC addition.

A high concentration of $Li_2O$ in the FEC-containing electrolyte suggests that the diffusion of HF (formed from fluorinated compounds) through the SEI is prevented. Note that $Li_2O$ is a reaction product of the successive decomposition of the native $SiO_2$ layer on silicon with the electrolyte in the first cycle. The additive-free electrolyte causes high electrolyte decomposition and shows no ability to prevent dissolution of $Li_2O$. Phosphorus species seem to play a negligible role in the additive-free electrolyte. In contrast, high concentrations of phosphate are observed with FEC addition which may result from an increased amount of water traces. The water traces are attributed to a higher HF release from the fluorinated additive and its subsequent reaction with oxides and carbonates ($SiO_2$, $Li_2O$, $Li_2CO_3$). Our results suggest that both the FEC and the $SiO_2$ play a critical role in the reversibility of silicon-based anodes. The application of another binder does not completely change the overall structure of the SEI, but it can complicate the analysis due to the occurrence of more electrolyte-related components on the surface caused by swelling effects or a stronger interaction with the PAA binder. Fig. 9 illustrates a simplified schematic view of the silicon–carbon nanostructure before and after cycling depending on FEC addition.

## Acknowledgements

## References

1 P. G. Bruce, S. A. Freunberger, L. J. Hardwick and J.-M. Tarascon, *Nat. Mater.*, 2012, **11**, 19–30.

2 J.-M. Tarascon and M. Armand, *Nature*, 2001, **414**, 359–367.

3 C.-M. Park, J.-H. Kim, H. Kim and H.-J. Sohn, *Chem. Soc. Rev.*, 2010, **39**, 3115–3141.

4 J. Brückner, S. Thieme, F. Böttger-Hiller, I. Bauer, H. T. Grossmann, P. Strubel, H. Althues, S. Spange and S. Kaskel, *Adv. Funct. Mater.*, 2014, **24**(9), 1284.

5 J. Balach, T. Jaumann, M. Klose, S. Oswald, J. Eckert and L. Giebeler, *J. Phys. Chem. C*, 2015, **119**(9), 4580.

6 Y. Yang, M. T. McDowell, A. Jackson, J. J. Cha, S. S. Hong and Y. Cui, *Nano Lett.*, 2010, **10**, 1486–1491.

7 D. Aurbach, *J. Power Sources*, 2000, **89**, 206–218.

8 H. Wu, G. Chan, J. W. Choi, I. Ryu, Y. Yao, M. T. McDowell, S. W. Lee, A. Jackson, Y. Yang, L. Hu and Y. Cui, *Nat. Nanotechnol.*, 2012, **7**, 310–315.

9 N. Liu, H. Wu, M. T. McDowell, Y. Yao, C. Wang and Y. Cui, *Nano Lett.*, 2012, **12**, 3315–3321.

10 H. Kim, M. Seo, M.-H. Park and J. Cho, *Angew. Chem., Int. Ed.*, 2010, **49**, 2146–2149.

11 J. Song, S. Chen, M. Zhou, T. Xu, D. Lv, M. L. Gordin, T. Long, M. Melnyk and D. Wang, *J. Mater. Chem. A*, 2014, **2**, 1257–1262.

12 T. Jaumann, M. Herklotz, M. Klose, K. Pinkert, S. Oswald, J. Eckert and L. Giebeler, *Chem. Mater.*, 2015, **27**, 37–43.

13 N.-S. Choi, K. H. Yew, K. Y. Lee, M. Sung, H. Kim and S.-S. Kim, *J. Power Sources*, 2006, **161**, 1254–1259.

14 B. Philippe, R. Dedryvère, M. Gorgoi, H. Rensmo, D. Gonbeau and K. Edström, *J. Am. Chem. Soc.*, 2013, **135**, 9829–9842.

15 S. Dalavi, P. Guduru and B. L. Lucht, *J. Electrochem. Soc.*, 2012, **159**, A642–A646.

16 Y.-M. Lin, K. C. Klavetter, P. R. Abel, N. C. Davy, J. L. Snider, A. Heller and C. B. Mullins, *Chem. Commun.*, 2012, **48**, 7268–7270.

17 X. Chen, X. Li, D. Mei, J. Feng, M. Y. Hu, J. Hu, M. Engelhard, J. Zheng, W. Xu, J. Xiao, J. Liu and J.-G. Zhang, *ChemSusChem*, 2014, **7**, 549–554.

18 A. Bordes, K. Eom and T. F. Fuller, *J. Power Sources*, 2014, **257**, 163–169.

19 V. Etacheri, O. Haik, Y. Goffer, G. A. Roberts, I. C. Stefan, R. Fasching and D. Aurbach, *Langmuir*, 2012, **28**, 965–976.

20 H. Nakai, T. Kubota, A. Kita and A. Kawashima, *J. Electrochem. Soc.*, 2011, **158**, A798–A801.

21 J. S. Kim, D. Byun and J. K. Lee, *Curr. Appl. Phys.*, 2014, **14**, 596–602.

22 R. Elazari, G. Salitra, G. Gershinsky, A. Garsuch, A. Panchenko and D. Aurbach, *J. Electrochem. Soc.*, 2012, **159**, A1440–A1445.

23 I. A. Profatilova, C. Stock, A. Schmitz, S. Passerini and M. Winter, *J. Power Sources*, 2013, **222**, 140–149.

24 B. Philippe, R. Dedryvère, J. Allouche, F. Lindgren, M. Gorgoi, H. Rensmo, D. Gonbeau and K. Edström, *Chem. Mater.*, 2012, **24**, 1107.

25 B. Philippe, R. Dedryvère, M. Gorgoi, H. Rensmo, D. Gonbeau and K. Edström, *Chem. Mater.*, 2013, **25**, 394–404.

26 K. Schroder, J. Alvarado, T. A. Yersak, J. Li, N. Dudney, L. J. Webb, Y. S. Meng and K. J. Stevenson, *Chem. Mater.*, 2015, **27**, 5531–5542.

27 K. W. Schroder, H. Celio, L. J. Webb and K. J. Stevenson, *J. Phys. Chem. C*, 2012, **116**, 19737–19747.

28 C. Pereira-Nabais, J. Światowska, A. Chagnes, A. Gohier, S. Zanna, A. Seyeux, P. Tran-Van, C.-S. Cojocaru, M. Cassir and P. Marcus, *J. Phys. Chem. C*, 2014, **118**, 2919–2928.

29 R. Dedryvère, L. Gireaud, S. Grugeon, S. Laruelle, J.-M. Tarascon and D. Gonbeau, *J. Phys. Chem. B*, 2005, **109**, 15868–15875.

30 K. Tasaki, A. Goldberg, J.-J. Lian, M. Walker, A. Timmons and S. J. Harris, *J. Electrochem. Soc.*, 2009, **156**, A1019–A1027.

31 J.-S. Bridel, T. Azaïs, M. Morcrette, J.-M. Tarascon and D. Larcher, *Chem. Mater.*, 2010, **22**, 1229–1241.

32 A. Xiao, L. Yang, B. L. Lucht, S.-H. Kang and D. P. Abraham, *J. Electrochem. Soc.*, 2009, **156**(4), A318–A327.

33 S.-H. Kang, D. P. Abraham, A. Xiao and B. L. Lucht, *J. Power Sources*, 2008, **175**, 526–532.

34 A. Magasinski, B. Zdyrko, I. Kovalenko, B. Hertzberg, R. Burtovyy, C. F. Huebner, T. F. Fuller, I. Luzinov and G. Yushin, *ACS Appl. Mater. Interfaces*, 2010, **2**, 3004–3010.

24966 | *Phys. Chem. Chem. Phys.*, 2015, **17**, 24956–24967

This journal is © the Owner Societies 2015

35  S. Oswald, *Appl. Surf. Sci.*, 2015, **351**, 492–503.

36  W. J. I. DeBenedetti and Y. J. Chabal, *J. Vac. Sci. Technol., A*, 2013, **31**, 050826.

37  M. L. Mastronardi, E. J. Henderson, D. P. Puzzo, Y. Chang, Z. B. Wang, M. G. Helander, J. Jeong, N. P. Kherani, Z. Lu and G. A. Ozin, *Small*, 2012, **8**, 36–47.

38  Y. Yu, C. M. Hessel, T. D. Bogart, M. G. Panthani, M. R. Rasch and B. A. Korgel, *Langmuir*, 2013, **29**, 1533–1540.

39  H. Wu, G. Yu, L. Pan, N. Liu, M. T. McDowell, Z. Bao and Y. Cui, *Nat. Commun.*, 2013, **4**, 1943.

40  C. Xu, F. Lindgren, B. Philippe, M. Gorgoi, F. Björefors, K. Edström and T. Gustafsson, *Chem. Mater.*, 2015, **27**, 2591–2599.

41  D. Aurbach, B. Markovsky, I. Weissman, E. Levi and Y. Ein-Eli, *Electrochim. Acta*, 1999, **45**, 67–86.

42  J. Li and J. R. Dahn, *J. Electrochem. Soc.*, 2007, **154**, A156–A161.

43  K. Xu, *Chem. Rev.*, 2014, **114**, 11503–11618.

44  Z. Chen and K. Amine, *J. Electrochem. Soc.*, 2006, **153**, A1221–A1225.

45  N. Azimi, W. Weng, C. Takoudis and Z. Zhang, *Electrochem. Commun.*, 2013, **37**, 96–99.

46  H. Kim, F. Wu, J. T. Lee, N. Nitta, H.-T. Lin, M. Oschatz, W. I. Cho, S. Kaskel, O. Borodin and G. Yushin, *Adv. Energy Mater.*, 2014, 1401792.

47  K. László, K. Josepovits and E. Tombácz, *Anal. Sci.*, 2001, **17**, i1741–i1746.

48  K. Ciosek Högström, S. Malmgren, M. Hahlin, H. Rensmo, F. Thebault, P. Johansson, K. Edström, M. Armand and J.-M. Tarascon, *J. Phys. Chem. C*, 2013, **117**, 23476–23486.

49  L. Martin, H. Martinez, M. Ulldemolins, B. Pecquenard and F. Le Cras, *Solid State Ionics*, 2012, **215**, 36–44.

50  M. Hoffmann, M. Zier, S. Oswald and J. Eckert, *J. Power Sources*, 2015, **288**, 434–440.

51  S. Sim, P. Oh, S. Park and J. Cho, *Adv. Mater.*, 2013, **25**, 4498–4503.

This journal is © the Owner Societies 2015

*Phys. Chem. Chem. Phys.*, 2015, **17**, 24956–24967  |  **24967**